Appl. Math. J. Chinese Univ.
2022, 37(3): 366-382

MHD stagnation point flow of nanofluid with SWCNT and MWCNT over a stretching surface driven by Arrhenius kinetics

Sohail Nadeem[1,*] Shafiq Ahmad[1]
Alibek Issakhov[2] Ibrahim M. Alarifi[3]

Abstract. The intention of the current research is to address the conclusion of non-isothermal heterogeneous reaction on the stagnation – point flow of SWCNT – engine oil and MWCNT – engine oil nanofluid over a shrinking/stretching sheet. Further, exemplify the aspect of heat and mass transfer the upshot of magnetohydrodynamics (MHD), thermal radiation, and heat generation/absorption coefficient are exemplified. The bvp4c from Matlab is pledged to acquire the numerical explanation of the problem that contains nonlinear system of ordinary differential equations (ODE). The impacts of miscellaneous important parameters on axial velocity, temperature field, concentration profile, skin friction coefficient, and local Nusselt number, are deliberated through graphical and numerically erected tabulated values. The solid volume fraction diminishes the velocity distribution while enhancing the temperature distribution. Further, the rate of shear stress declines with increasing the magnetic and stretching parameter for both SWCNT and MWCNT.

§1 Introduction

Numerous chemically reacting systems include both heterogeneous and homogeneous reactions, with precedents happening in catalysis, biochemical, and combustion systems. The cooperation among the heterogeneous and homogeneous reactions is extremely intricate including the invention and utilization of reactant species at various rates both within the fluid and on the catalytic sheets, for example, hydro metallurgical industry, reactions happening in food processing, polymer production and manufacturing of ceramics, dispersion and fog formation,

Received: 2019-11-20. Revised: 2020-07-29.
MR Subject Classification: 76D10, 76W05.
Keywords: heat generation, surface reaction, CNTs based nanofluid, stretching/shrinking sheet, thermal radiation.
Digital Object Identifier(DOI): https://doi.org/10.1007/s11766-022-3966-z.
*Corresponding author.

crops damage through freezing, temperature distribution and cooling towers and forests of fruit trees and dampness over agricultural fields. Merkin [1] explored the model of isothermal heterogeneous and homogeneous reactions in the boundary layer flow through a flat plate. The stagnation-point boundary-layer flow in the sight of heterogeneous – homogeneous reaction discussed by Chaudhary and Merkin [2]. Mahdy [3] discretized the boundary layer flow via a vertical permeable cone with heterogeneous – homogeneous reaction. Xu [4] explained the Blasius flow in the existence of heterogeneous – homogeneous reaction. Nadeem et al. [5] scrutinized the ferrofluid via a stretching cylinder in the occurrence of heterogeneous – homogeneous reaction. In the last year, many researchers discussed the importance of heterogeneous – homogeneous reaction [6-9].

Engineered suspension of nanoparticles in fluids (for example, ethylene glycol, water, and oil) known as "nano fluids" has picked up considerable interest because of their improved thermal conductivity. The nanoparticles (nanometer-sized particles) utilized in nanofluids are regularly made of carbon nanotubes, metals, oxides or carbides. Nanofluids have narrative properties that make them conceivably helpful in numerous applications in heat transfer, containing fuel cells, hybrid-powered engines, microelectronics and pharmaceutical processes, domestic refrigerator, engine cooling/vehicle thermal management, machining, chiller, heat exchanger, in grinding and in boiler flue gas temperature reduction. Choi [10] initially utilized the nanoparticles to upgrade the thermal conductivity of liquids and storage of energy. Nadeem [11] study steady nanofluid boundary layer flow through a wedge. Khan and Pop [12] numerically investigate the nanofluid flow past a stretching sheet. Heris et al. [13] considered the circular tube to examine the transfer of heat in two phase nanofluid experimentally. Li [14] discussed the flow attribute of Cu – water nanofluid and convective heat transfer. Recently many researchers study the boundary layer flow for different nanofluids [15-20].

Because of the vast application of stagnation point flow in the natural phenomena, industry processes, and engineering, scientists and researchers are intrigued to investigate the attributes of flow performance in the area of stagnation point (i.e., oblique and orthogonal stagnation point). Fluid motion in the area of a stagnation point occurs on all moving solid bodies. Hiemenz [21] was the first who concentrated on two-dimensional stagnation point flow over a stretching sheet. Akbar et al. [22] studied the CNTs nanofluid stagnation point flow with convective boundary condition past a stretching sheet. Iqbal et al. [23] discussed the stagnation point flow with induced magnetic field and CNTs. Hayat et al. [24] examined the heterogeneous – homogeneous reaction in the CNTs nanoparticles on stagnation point flow in the existence of Newtonian heating. In the occurrence of CNTs the MHD slip flow along a stretching surface is discussed by Haq. [25].

Chaudhar and Merkin [26] and Merkin and Pop [27] examined the non-isothermal, one step reaction administered by Arrhenius kinetics. In this study, we extend the work of Merkin and Pop [27] by introducing the effect of nanoparticles SWCNT and MWCNT with engine oil taken as base fluid. Moreover, the influence of magnetohydrodynamics (MHD), thermal radiation, and heat generation is incorporated to study the silent feature of heat and mass

transfer. The numerical scheme called bvp4c function from MATLAB is discretized to explain the nonlinear ordinary differential equations (ODE). The influence of various parameters is shown graphically and numerical values on shear heat transfer (skin friction), Nusselt number (Nu_x), and concentration on surface.

§2 Modeling of constitutive equations

The steady, incompressible two-dimensional stagnation point flow on a stretching/shrinking surface are considered. The energy equation is carried out in the existence of heat generation/absorption coefficient, linear thermal radiation, and catalytic surface heating. Two type of nanoparticles SWCNT and MWCNT are taken into account with engine oil is a base fluid. Here u and v are the velocity components. Cartesian coordinate taken along the flow and normal to it. The flow is initiate because of extending or contracting of the sheet caused by the concurrent application of two equivalent forces through the x-axis. It is accepted that U_w is the velocity of the shrinking/stretching surface. A uniform magnetic field of strength B_0 is applied in the y- direction. We consider the non-isothermal heterogenous reaction administrated by Arrhenius energy of the form [26, 27]

$$A \to B \qquad \text{rate} = k_0 a^* e^{-E_a/RT}. \tag{1}$$

Here A and B are the chemical species, T is temperature of fluid, E_a represent the activation energy, R demonstrate the gas constant, and k_0 is constant.

After using the boundary layer approximation, the continuity equation, momentum equation, temperature equation, and concentration equation take the form [27, 11]

$$\frac{\partial v}{\partial y} + \frac{\partial u}{\partial x} = 0, \tag{2}$$

$$v\frac{\partial u}{\partial y} + u\frac{\partial u}{\partial x} - U_\infty \frac{dU_\infty}{dx} = \frac{\mu_{nf}}{\rho_{nf}}\frac{\partial^2 u}{\partial y^2} - \frac{\sigma_{nf}{B_0}^2}{\rho_{nf}}(u - U_\infty), \tag{3}$$

$$v\frac{\partial T}{\partial y} + u\frac{\partial T}{\partial x} = \left(\alpha_{nf} + \frac{16\sigma^* {T_\infty}^3}{3k_f k^*}\right)\frac{\partial^2 T}{\partial y^2} + \frac{Q_0}{(\rho C_p)_{nf}}(T - T_\infty) \tag{4}$$

$$v\frac{\partial a^*}{\partial y} + u\frac{\partial a^*}{\partial x} = D^*\frac{\partial^2 a^*}{\partial y^2} \tag{5}$$

The appropriate boundary conditions are specified by:

$$\begin{aligned} &v = 0,\ u = U_w,\ k_{nf}\frac{\partial T}{\partial y} = -Qk_0 a^* e^{\frac{-E_a}{RT}},\ D^*\frac{\partial a^*}{\partial y} = k_0 a^* e^{\frac{-E_a}{RT}} \qquad \text{at} \qquad y = 0,\\ &u \to U_\infty,\ T \to T_\infty,\ a^* \to a^*_\infty \qquad \text{at} \qquad y = \infty. \end{aligned} \tag{6}$$

Here Eq. 2 demonstrate the continuity equation which shows that mass transfer is conserved, Eq. 3 derived from Navier–Stokes equations which study the linear momentum, Eq. 4 is the temperature equation which is derived from the Fourier's law of heat conduction and study the heat flux and Eq. 5 derived from Fick's laws to describe the mass concentration. Where $U_w = \lambda U_\infty$ and the far field velocity (inviscid flow) is $U_\infty = \frac{U_0 x}{l}$ and the reaction at rate $Qk_0 a^* e^{\frac{-E_a}{RT}}$ heat is released.

2.1 Thermo-physical properties of SWCNT-engine oil, MWCNTengine oil nanofluids

The specific heat, electrical conductivity, the dynamic viscosity, the effective dynamic densit, and the thermal conductivity of the nanofluid are disposed by Xue [28].

$$\begin{aligned}
&\frac{\mu_{nf}}{\mu_f} = (1-\phi)^{-2.5}, \rho_{nf} = (1-\phi)\rho_f + \phi\rho_{CNT},\\
&(\rho C_p)_{nf} = (1-\phi)(\rho C_p)_f + \phi(\rho C_p)_{CNT},\\
&\frac{k_{nf}}{k_f} = -\frac{(1-\phi) + 2\phi\frac{k_{CNT}}{k_{CNT}-k_f}\ln(\frac{k_{CNT}+k_f}{2k_f})}{(1-\phi) + 2\phi\frac{k_f}{k_{CNT}-k_f}\ln(\frac{k_{CNT}+k_f}{2k_f})},\\
&\frac{\sigma_{nf}}{\sigma_f} = 1 - \frac{3\phi[1-\frac{\sigma_{CNT}}{\sigma_f}]}{[2+\frac{\sigma_{CNT}}{\sigma_f}] + \phi[1-\frac{\sigma_{CNT}}{\sigma_f}]}
\end{aligned} \tag{7}$$

The numerical values of specific heat, density, and thermal conductivity of CNTs and engine oil are specified in Table 1 below.

Table 1. Thermophysical properties of the engine oil and the nanoparticles (SWCNT, MWCNT).

Physical properties	Base Fluid	Nanoparticles	
	Engine oil	MWCNTs	SWCNTs
C_p(J/kg K)	1910	796	425
ρ(kg/m^3	884	1600	2600
K(W/mK)	0.144	3000	6600

§3 Solution procedure

Consuming the non-dimensional and similarity transformations

$$\psi = \sqrt{\frac{U_\infty \nu_f}{l}} x f(\eta),\ \eta = \sqrt{\frac{U_\infty}{\nu_f l}} y,\ T - T_\infty = \frac{R{T_\infty}^2}{E_a}\theta(\eta),\ a^* - a^*{}_\infty = a^*{}_\infty g(\eta),$$

$$u = \frac{\partial\psi}{\partial y} = \frac{xU_\infty}{l} f'(\eta),\ v = -\frac{\partial\psi}{\partial x} = -\sqrt{\frac{U_\infty \nu_f}{l}} f(\eta). \tag{8}$$

These transformations directly satisfy Eq. 2 and Eqs. 3 to 6 yield the form

$$\frac{1}{(1-\phi)^{2.50}(1-\phi+\phi\frac{\rho_{CNT}}{\rho_f})} f''' + ff'' - f'^2 - M\frac{\sigma_{nf}/\sigma_f}{(1-\phi+\phi\frac{\rho_{CNT}}{\rho_f})}(f'-1) = 0 \tag{9}$$

$$\left(\frac{k_{nf}}{k_f} + Rd\right)\theta'' + \Pr\left[1-\phi+\phi\frac{(\rho C_p)_{CNT}}{(\rho C_p)_f}\right] f\theta' + \Pr\gamma\theta = 0 \tag{10}$$

$$\frac{1}{S_c} g'' + fg' = 0 \tag{11}$$

maintained by the boundary conditions

$$f(0)=0,\quad f'(0)=\lambda,\quad \frac{k_{nf}}{k_f}\theta'(0)=-\alpha\,(1+g(0))\,e^{\frac{\theta(0)}{1+\epsilon\theta(0)}},$$
$$g'(0)=\beta\,(1+g(0))\,e^{\frac{\theta(0)}{1+\epsilon\theta(0)}},$$
$$f'(\eta)\to 1,\quad \theta(\eta)\to 0,\quad g(\eta)\to 0\qquad \eta\to\infty. \tag{12}$$

where prime label the derivative with respect to η and the dimensionless involved parameter is defined as,

$$M=\frac{\sigma_f {B_0}^2}{U_\infty \rho_f}, R_d=\frac{16\sigma^* {T_\infty}^3}{3k_f k^*}, \gamma=\frac{Q_0 l}{(\rho C_p)_f U_\infty}, S_c=\frac{\upsilon_f}{D_A}, \alpha=\frac{QE_a {a^*}_\infty k_0 e^{\frac{-E_a}{RT_\infty}}}{k_f R{T_\infty}^2},$$
$$\Pr=\frac{\nu_f}{\alpha_f}, \varepsilon=\frac{RT_\infty}{E_a}, \beta=\frac{k_0 e^{\frac{-E_a}{RT_\infty}}}{D^*}\sqrt{\frac{\upsilon_f l}{U_\infty}}.$$

The physical quantity such as rate of shear stress (skin friction coefficient) and the rate of heat transfer (Nusselt number) as define as

$$C_f=\frac{\tau_w}{\rho_f U_\infty^2}\qquad Nu_x=\frac{xq_w}{k_f(T_f-T_\infty)},$$
$$\tau_w=\mu_{nf}(\frac{\partial u}{\partial y})_{y=o},\ q_w=-k_{nf}(\frac{\partial T}{\partial y})_{y=0}+(q_r)_w. \tag{13}$$

Consuming the similarity transformation (8) the above equations become

$$C_f\sqrt{Re_x}=(1-\phi)^{-2.5}f''(0), Nu_x[Re_x]^{-1/2}=-\left[\frac{k_{nf}}{k_f}+R_d\right]\theta'(0), \tag{14}$$

where the local Reynold number is $Re_x=\frac{xU_\infty(x)}{\upsilon_f}$.

3.1 Numerical method

The coupled equations (9–11) with corresponding condition (12) are numerically solved using BVP-4c function of MATLAB. Consuming new parameters the third and second order nonlinear differential equation change to first order ordinary differential equation. We have chosen the tolerance as 10^{-4} for this particular issue to fulfill the equation and the boundary conditions asymptotically. The first order system acquired in such manner is affixed beneath:

$$A=(1-\phi)^{2.5}(1-\phi+\phi\frac{\rho_{CNT}}{\rho_f}),\ B=(1-\phi+\phi\frac{\rho_{CNT}}{\rho_f}),$$
$$C=\left[1-\phi+\phi\frac{(\rho C_p)_{CNT}}{(\rho C_p)_f}\right],\ D=\frac{k_{nf}}{k_f}, \tag{15}$$
$$y(1)=f,\ y(2)=f',\ y(3)=f'',\ y(4)=\theta,\ y(5)=\theta',\ y(6)=g,\ y(7)=g'$$
$$yy1=f'''=-A\left\{y(1)y(3)+1-y(2)y(2)-M\frac{\sigma_{nf}/\sigma_f}{B}(y(2)-1)\right\},$$
$$yy2=\theta''=\frac{-1}{(D+R_d)}\left\{\Pr Cy(5)y(1)+\gamma\Pr y(4)\right\},$$
$$yy3=g''=-S_c y(1)y(7) \tag{16}$$

with conditions,

$$y_0(2) - \lambda = 0,\ Dy_0(5) + \alpha(1 + y_0(6))e^{\frac{y_0(4)}{1+\epsilon y_0(4)}}\ y_0(7) - \beta(1 + y_0(6))e^{\frac{y_0(4)}{1+\epsilon y_0(4)}} \tag{17}$$

$$y_0(1) = 0,\ y_\infty(2) - 1 = 0,\ y_\infty(4) = 0,\ y_\infty(6) = 0. \tag{18}$$

We have picked $\eta_\infty = 4$, that ensures each numerical solution's asymptotic value precisely.

§4 Results and discussion

Figs. (1-14) display the upshot of various appropriate parameters comprising nanoparticles volume fraction ($0 \leq \phi \leq 0.3$), magnetic parameter ($1 \leq M \leq 3$), heat generation/absorption coefficient ($0.1 \leq \gamma \leq 0.3$), radiation parameter ($0 \leq R_d \leq 2$), stretching/shrinking parameter ($\lambda = 0.3\text{and} - 0.3$), heat of reaction ($0.1 \leq \alpha \leq 0.5$), reaction rate constant ($0.1 \leq \beta \leq 0.5$), Prandtl number ($5 \leq \text{Pr} \leq 20$), and Schmidt number ($0.7 \leq S_c \leq 1.3$) on axial velocity, temperature profile, concentration field, skin friction coefficient, and local Nusselt number. The graphical results are discussed for both stretching and shrinking sheet. Fig. 1(a, b) and Fig. 2(a, b) demonstrate the effect of solid volume fraction ϕ of nanoparticle on axial velocity and temperature profile for both SWCNT and MWCNT. Fig. 1(a, b) shows that the velocity profile diminishes with enhancing the value of solid volume fraction ϕ. Physically, enhancement in ϕ the dynamic viscosity and density of nanofluid enhances as a result axial velocity diminishes. It is also recommended that for shrinking surface $\lambda > 0$ axial velocity rapidly decreases with compare stretching sheet $\lambda > 0$ in both CNTs – engine oil. The temperature profile is the increasing function of solid volume fraction ϕ for both stretching/shrinking sheet, while near the surface it decreases display in Fig. 2(a, b). Fig. 3(a) depict that for SWCNT-engine oil the axial velocity enhances with enhancing the value of magnetic parameter M for $\lambda > 0$ and $\lambda > 0$. Also, for MWCNT- engine oil boost magnetic parameter M the velocity profile enhances while their corresponding momentum boundary layer thickness decreases for both stretching and shrinking sheet which is define in Fig. 3(b). Fig. 4(a) and 4(b) delineates the feature of αon temperature distribution in SWCNT-engine oil and MWCNT-engine oil correspondingly. The increment is found in temperature profile with enhancing α. It is also seen that the thermal boundary layer thickness is higher for shrinking sheet $\lambda > 0$ is compared to stretching sheet $\lambda > 0$. Fig. 5(a, b) demonstrate that the temperature profile boosts with boosting the value of radiation parameter R_d for both stretching and shrinking sheet. This is based on the fact that under influence of R_d the surface heat flux improves which results in increased temperature within the boundary layer area In Fig. 6(a) the performance of Prandtl number on temperature profile is examined. We saw that temperature penetration depth is astonishingly greater at Pr = 10, while contrasted and Pr = 20. Physically, Pr and thermal diffusivity is an inverse relation, so rate of thermal diffusion is slow while enhancing the Prandtl number Pr. Subsequently an upgrade in Pr decreases conduction and because of this reality the penetration depth of temperature is likewise diminishes. Further the thermal boundary layer thickness closed to surface speedy for stretching sheet than shrinking sheet. Similarly, behavior will be found for

MWCNT-engine oil assumed in Fig. 6(b). Fig. 7(a) and Fig. 7(b) respectively scrutinized the temperature distribution for SWCNT-engine oil and MWCNT-engine oil with increasing the heat generation/absorption coefficient. The improvement in temperature field will be perceived with rising the heat generation/absorption coefficient. Also, the thermal boundary layer thickness is smaller for stretching sheet ($\lambda > 0$) is compared to shrinking sheet ($\lambda < 0$). Fig. 8(a, b) exhibit the variation of Schmidt number S_c on concentration filed for SWCNT-engine oil and MWCNT-engine oil with along stretching and shrinking sheet. Concentration profile is the enhancing function of Schmidt number S_c. Indeed, the Schmidt number S_c is the proportion of force diffusivity to mass diffusivity, so small diffusivity relates to larger Schmidt number S_c. Thus, concentration filed enhances while their corresponding concentration boundary layer thickness diminishes. Lower the concentration profile with larger the reaction rate constant β for both SWCNT and MWCNT which is given in Figs. 9(a, b). While the concentration boundary layer thickness enhances for larger value of β for both stretching surface and shrinking surface. Figs. 10(a, b) illustrate the concentration profile for boosting values of heat of reaction parameter α in SWCNT and MWCNT. The concentration profile diminishes with increasing heat of reaction parameter α. It is also seen that the concentration boundary layer thickness is higher for shrinking sheet than stretching sheet. Fig. 11 conclude the effect of magnetic parameter via stretching/shrinking parameter on skin friction profile for SWCNT and MWCNT with base fluid engine oil. Skin friction diminishes with enhancing magnetic parameter. Also, for stretching parameter $\lambda > 0$ the skin friction decreases while for shrinking sheet $\lambda > 0$ the rate of shear stress enhances. Skin friction is an increasing function of magnetic parameter while it is decrease with boosting λ for both CNTs which is define in Fig. 12. Fig. 13 demonstrate the rate of heat transfer for SWCNT and MWCNT with boosting value of radiation parameter R_d and heat of reaction parameter α over a Prandtl number Pr. It is gotten that the rate of heat transfer (skin friction) upgrades with rising the significance of radiation parameter (R_d), heat of reaction parameter (α), and Prandtl number (Pr). The rate of heat transfer (Nusselt number) reduce with evaluate the magnetic parameter via heat generation/absorption parameter for both CNTs is depict in Fig. 15. Fig. 16 show that the rate of heat transfer enhances with growing the heat of reaction parameter α with respect to radiation parameter R_d for both SWCNT and MWCNT as engine oil is a base fluid. Fig. 14 illustrate the flow streamline for changing value of stretching/shrinking parameter λ. Table. 2 communicate the numerical values of the rate shear stress (skin friction) for changing parameter with SWCNT and MWCNT. It is found that the shear stress enhances for enhancing the solid volume fraction (ϕ) and magnetic parameter (M) while it is diminishes for enlarging value of stretching parameter (λ). Table. 3 manifest the numerical value of Nusselt number for innumerable parameter with SWCNT and MWCNT. It is detected that the numerical value of Nusselt number enhances for magnetic parameter M, heat of reaction parameter α, and radiation parameter R_d while diminishes for solid volume fraction ϕ, and heat generation/absorption coefficient γ.

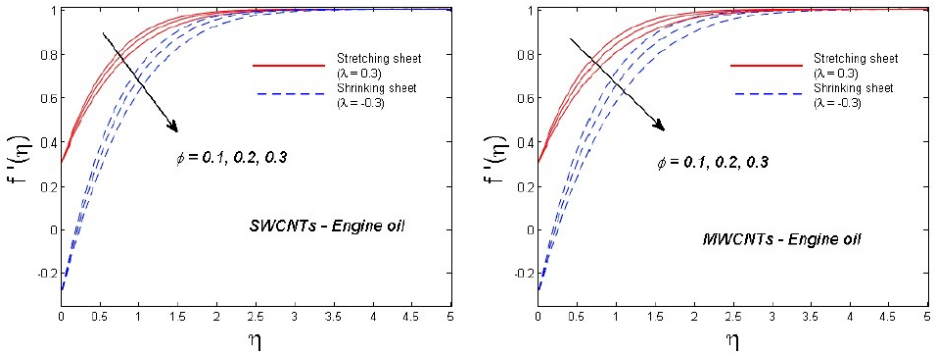

Figure 1. Effect of solid volume fraction ϕ on axial velocity for SWCNT and MWCNT.

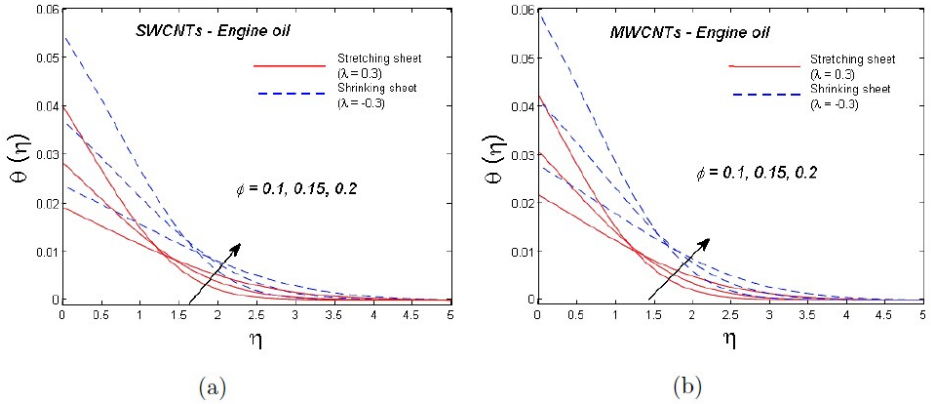

Figure 2. Effect of solid volume fraction ϕ on temprature profile for SWCNT and MWCNT.

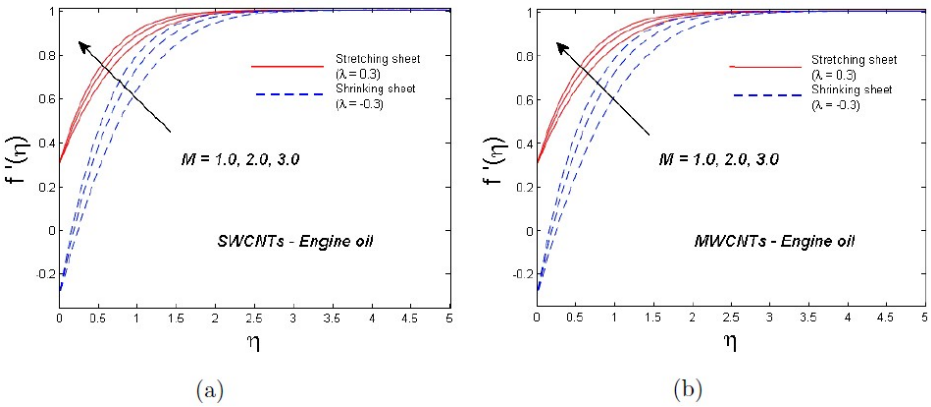

Figure 3. Action of magnetic parameter M on velocity profile for SWCNT and MWCNT.

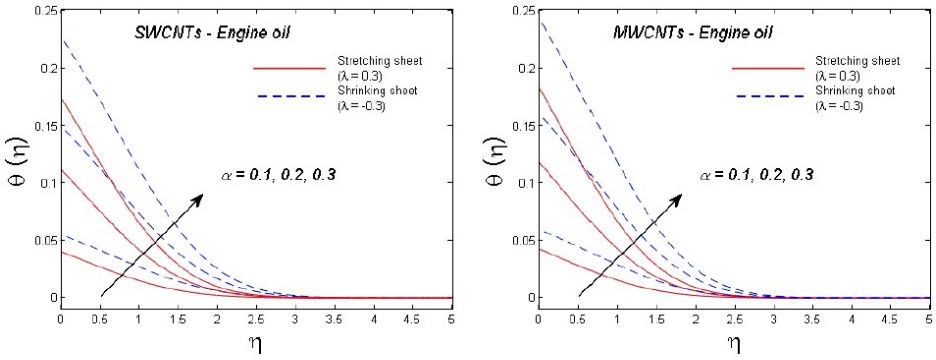

(a) (b)

Figure 4. Upshot of heat of reaction α on temprature profile for SWCNT and MWCNT.

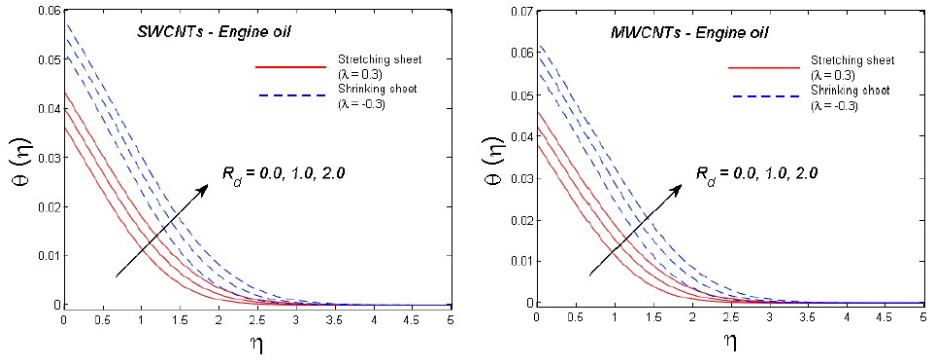

(a) (b)

Figure 5. Consequence of radiation parameter R_d on temperature profile for SWCNT and MWCNT.

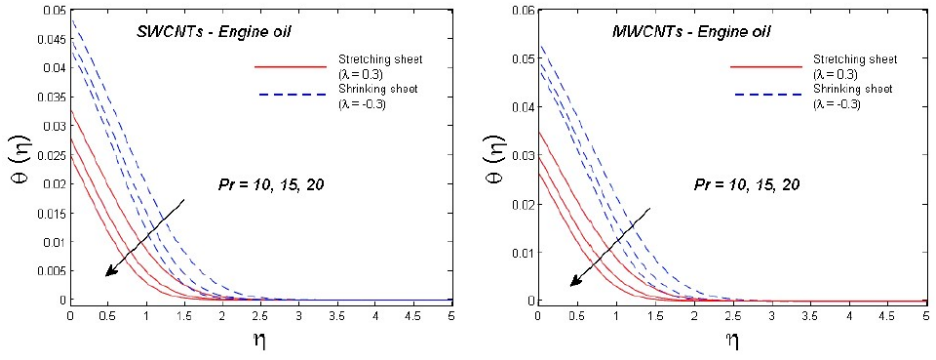

(a) (b)

Figure 6. Result of Prandtl number Pr on temprature field for SWCNT and MWCNT.

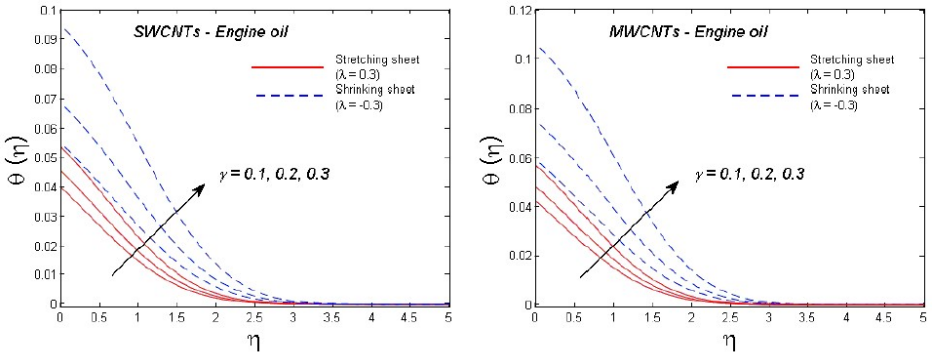

Figure 7. Influence of heat generation/absorption coefficient γ on temperature profile for SWCNT and MWCNT.

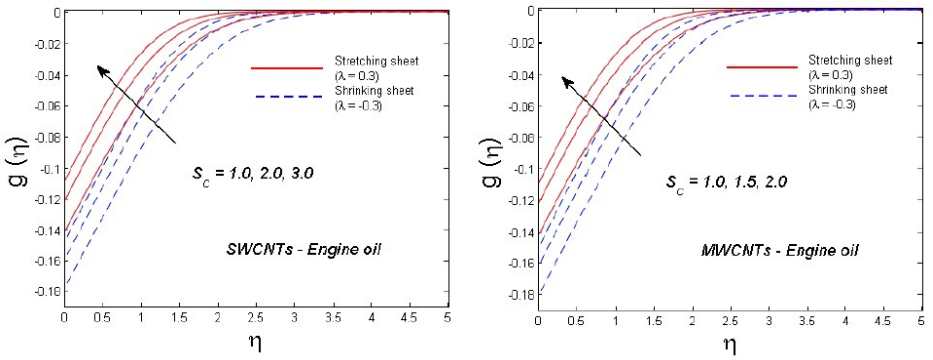

Figure 8. Effect of Schmidth number S_c on concentration profile for SWCNT and MWCNT.

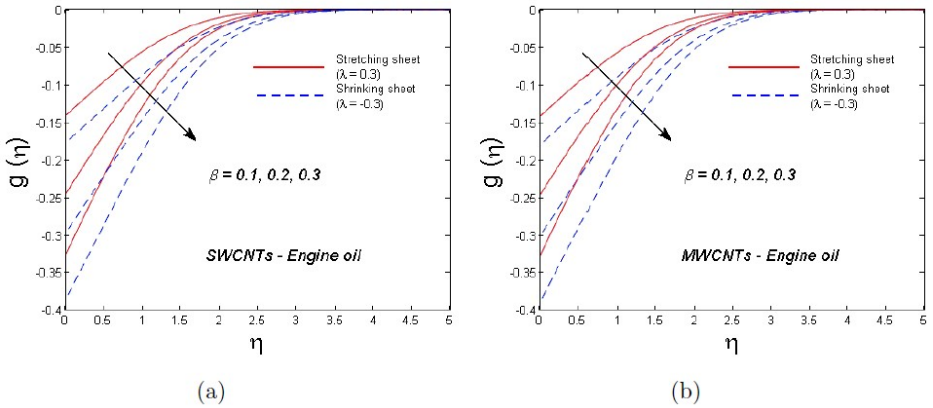

Figure 9. Effect of rection rate constant β on concenteration profile for SWCNT and MWCNT.

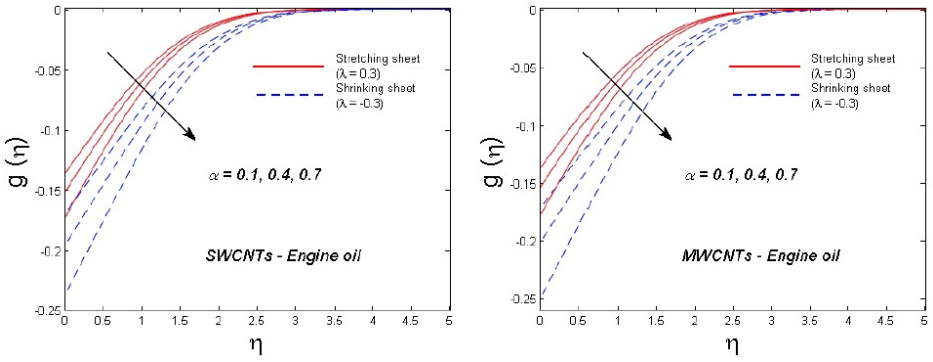

(a) (b)

Figure 10. Influence of α on concenteration profile for SWCNT and MWCNT.

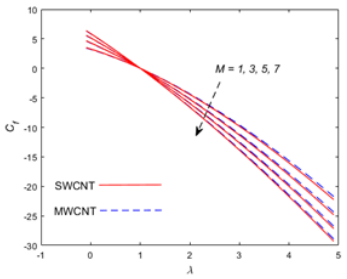

Figure 11. Influence of magnetic paramter M on Skin friction for SWCNT and MWCNT.

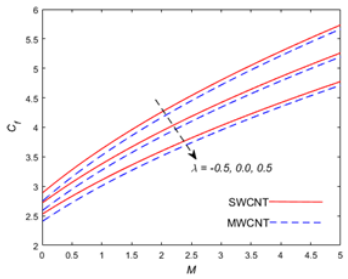

Figure 12. Impact of streching parameter λ on Skin friction for SWCNT and MWCNT.

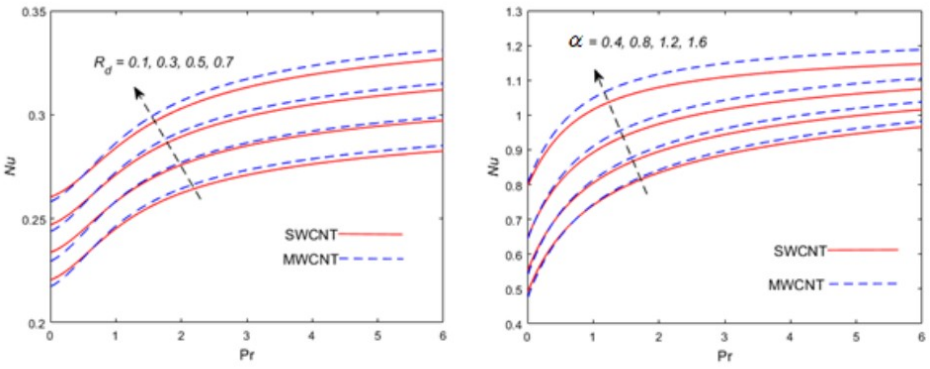

(a) (b)

Figure 13. Inspiration of radiation parameter R_d and heat of reaction parameter α on Nusselt number for SWCNT and MWCNT.

Table 2. Numerical value of skin friction for Engine oil base fluid with fixed value of $Sc = 0.1$, and $\Pr = 6.2$.

ϕ	M	λ	$[Re_x]^{1/2}C_f$	
			SWCNTs	MWCNTs
0.1	1.0	0.3	1.4229	1.3759
0.2			1.7383	1.6333
0.3			2.1549	1.9754
	1.0		1.4229	1.3759
	2.0		1.6306	1.5898
	3.0		1.8150	1.7785
		0.1	1.7576	1.7017
		0.2	1.5946	1.5428
		0.3	1.4229	1.3759

Table 3. Numerical value of Nusselt number for Engine oil base fluid with fixed value of $Sc = 0.1$ and $\Pr = 6.2$.

ϕ	M	α	γ	R_d	$[Re_x]^{-1/2}Nu_x$	
					SWCNTs	MWCNTs
0.1	1.0	0.1	0.1	1.0	0.12245	0.12473
0.2					0.10574	0.10732
0.3					0.09952	0.10009
	1.0				0.12245	0.12473
	2.0				0.12253	0.12482
	3.0				0.12258	0.12488
		0.2			0.23658	0.24056
		0.4			0.44288	0.44884
		0.6			0.62404	0.63056
			0.2		0.12183	0.12405
			0.4		0.12093	0.12150
			0.6		0.11950	0.11082
				0.3	0.10421	0.10476
				0.5	0.10942	0.11047
				0.7	0.11463	0.11617

§5 Conclusion

The idea of non-isothermal heterogenous reaction with stagnation point flow past a stretching/shrinking sheet in the presence of two different nanoparticle namely single wall carbon nanotube (SWCNT) and multi wall carbon nanotube (MWCNT) are examined. In the existence of linear thermal radiation and convective boundary the energy equation is carried out. The finite-difference-based numerical technique, specifically, bv4c is actualized the numerical solution of the nonlinear coupled equation. The sundry parameters effects show graphically for both stretching and shrinking sheet with SWCNT and MWCNT,

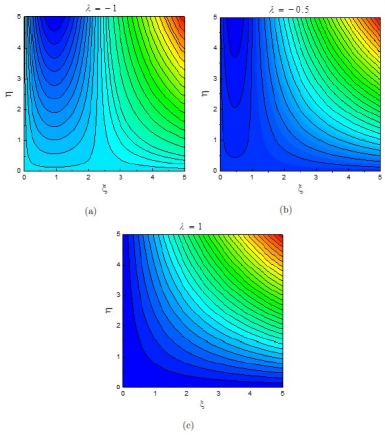

Figure 14. Flow streamlines for numerous values of stretching parameter λ.

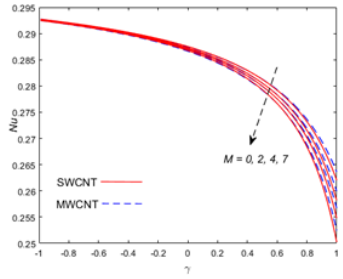

Figure 15. Motivation of magnetic parameter M on Nusselt number for SWCNT and MWCNT.

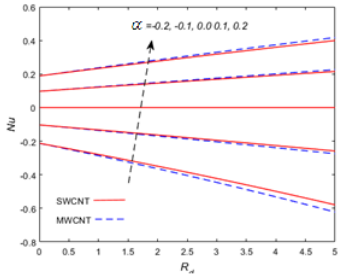

Figure 16. Impact of streching parameter λ on Skin friction for SWCNT and MWCNT.

The imperative findings of existing study are quantified below:

1. The axial velocity diminishes, and temperature field enhances in nature for boosting value of nanoparticle solid volume fraction.

2. Temperature distribution is an increasing function of α and radiation parameter for both stretching sheet $\lambda > 0$ and shrinking sheet $\lambda > 0$.

3. Larger the Schmidt number the concentration field increases for both SWCNTs and MWCNTs.

4. Radiation parameter and heat of reaction parameter α increases the rate of heat transfer, while decreases by magnetic parameter.

5. The rate of shear stress declines with swelling the magnetic parameter and stretching parameter for both CNTs.

Nomenclature

B_0	magnetic field of strength
v	along y-axis velocity component
C_p	Specific heat
U_w	stretching velocity along x-direction
C_f	surface drag force
U_∞	free stream velocity of the fluid
D^*	diffusion coefficients
u	along x-axis velocity component
f	dimensionless stream function
T,T_∞	temperature
k^*	mean absorption coefficient
S_c	Schmidt number
k_f, k_{nf}	thermal conductivity
Re_x	local Reynold number
Nu_x	Nusselt number
R_d	Radiation parameter
Pr	Prandtl number
R	gas constant
Q	heat of reaction
$q_w(x)$	the surface heat flux of nanoliquid film
Q_0	volumetric rate of heat source
ϕ	solid volume fraction of nanofluid
Greek symbols	
α	Dimensionless heat of reaction
α_{nf}	modified thermal diffusivity
β	Reaction rate constant
ψ	stream function
σ^*	Stephan-Boltzmann constant
μ_{nf}, μ_f	dynamic viscosity
τ_{xy}	shear stress
ρ_{CNT}, ρ_f	density
ϕ	solid volume fraction of nanofluid
$(\rho C_p)_{CNT}$,$(\rho C_p)_f$	heat capacity
θ	dimensionless temperature
λ	stretching/shrinking parameter
λ	stretching/shrinking parameter
η	a scaled boundary-layer coordinate
γ	dimensionless heat generation parameter

References

[1] J H Merkin. *A model for isothermal homogeneous-heterogeneous reactions in boundary-layer flow*, Math Comput Model, 1996, 24(8): 125-136.

[2] M A Chaudhary, and J H Merkin. *A simple isothermal model for homogeneous-heterogeneous reactions in boundary-layer flow. I Equal diffusivities*, Fluid Dyn Res, 1995, 16(6): 311.

[3] A Mahdy. *Aspects of homogeneous-heterogeneous reactions on natural convection flow of micropolar fluid past a permeable cone*, Appl Math Comput, 2019, 352: 59-67.

[4] H Xu. *Homogeneous–Heterogeneous Reactions of Blasius Flow in a Nanofluid*, J Heat Transfer, 2019, 141(2): 024501.

[5] S Nadeem, N Ullah, A U Khan, T Akbar. *Effect of homogeneous-heterogeneous reactions on ferrofluid in the presence of magnetic dipole along a stretching cylinder*, Results Phys, 2017, 7: 3574-3582.

[6] S Nadeem, S Ahmad, N Muhammad, M T Mustafa. *Chemically reactive species in the flow of a Maxwell fluid*, Results Phys, 2017, 7: 2607-2613.

[7] M Khan, L Ahmad, M Ayaz. *Numerical simulation of unsteady 3D magneto-Sisko fluid flow with nonlinear thermal radiation and homogeneous–heterogeneous chemical reactions*, Pramana, 2018, 91(1): 13.

[8] M Ramzan, S Ahmad, D Lu. *Numerical simulation for homogeneous-heterogeneous reactions and Newtonian heating in the silver-water nanofluid flow past a nonlinear stretched cylinder*, Phys Scr, 2019, 94(8): 085702.

[9] M M Bhatti, R Ellahi, A Zeeshan, M Marin, N Ijaz. *Numerical study of heat transfer and Hall current impact on peristaltic propulsion of particle-fluid suspension with compliant wall properties*, Mod Phys Lett B, 2019, 33(35): 1950439.

[10] S U S Choi, J A Eastman. *Enhancing thermal conductivity of fluids with nanoparticles*, No. ANL/MSD/CP-84938; CONF-951135-29. Argonne National Lab, IL (United States), 1995.

[11] S Nadeem, S Ahmad, and N Muhammad. *Computational study of Falkner-Skan problem for a static and moving wedge*, Sens Actuators B: Chem, 2018, 263: 69-76.

[12] W A Khan, and I Pop. *Boundary-layer flow of a nanofluid past a stretching sheet*, Int J Heat Mass Tran, 2010, 53(11-12): 2477-2483.

[13] S Z Heris, M N Esfahany, and S Gh Etemad. *Experimental investigation of convective heat transfer of Al_2O_3/water nanofluid in circular tube*, Int J Heat Fluid Fl, 2007, 28(2): 203-210.

[14] Q Li, Y Xuan. *Convective heat transfer and flow characteristics of Cu-water nanofluid*, Sci China Ser E: Technol Sci, 2002, 45(4): 408-416.

[15] S Nadeem, T Hayat, A U Khan. *Numerical study on 3D rotating hybrid SWCNT-MWCNT flow over a convectively heated stretching surface with heat generation/absorption*, Phys Scr, 2019, 94(7): 075202.

[16] A Sarlak, A Ahmadpour, M R Hajmohammadi. *Thermal design improvement of a double-layered microchannel heat sink by using multi-walled carbon nanotube (MWCNT) nanofluids with non-Newtonian viscosity*, Appl Therm Eng, 2019, 147: 205-215.

[17] A Hussanan, I Khan, M R Gorji, W A Khan. *CNT S-Water–Based Nanofluid Over a Stretching Sheet*, BioNanoScience 2019, 9(1): 21-29.

[18] N Muhammad, and S Nadeem. *Ferrite nanoparticles* $Ni - ZnFe_2O_4$, $Mn - ZnFe_2O_4$ *and* Fe_2O_4 *in the flow of ferromagnetic nanofluid*, Eur Phys J Plus, 2017, 132(9): 377.

[19] L Zhang, M B Arain, M M Bhatti, A Zeeshan, H Hal-Sulami. *Effects of magnetic Reynolds number on swimming of gyrotactic microorganisms between rotating circular plates filled with nanofluids*, Appl Math Mech-Engl, 2020, 41(4): 637-654.

[20] M M Bhatti, A Shahid, T Abbas, S Z Alamri, R Ellahi. *Study of activation energy on the movement of gyrotactic microorganism in a magnetized nanofluids past a porous plate*, Processes, 2020, 8(3): 328.

[21] K Hiemenz. *Die Grenzschicht an einem in den gleichformigen Flussigkeitsstrom eingetauchten geraden Kreiszylinder*, Dinglers Polytech. J, 1911, 326: 321-324.

[22] N S Akbar, Z H Khan, S Nadeem. *The combined effects of slip and convective boundary conditions on stagnation-point flow of CNT suspended nanofluid over a stretching sheet*, J Mol Liq, 2014, 196: 21-25.

[23] Z Iqbal, E Azhar, E N Maraj. *Transport phenomena of carbon nanotubes and bioconvection nanoparticles on stagnation point flow in presence of induced magnetic field*, Physica E Low Dimens Syst Nanostruct, 2017, 91: 128-135.

[24] T Hayat, M Farooq, A Alsaedi. *Homogeneous-heterogeneous reactions in the stagnation point flow of carbon nanotubes with Newtonian heating*, AIP Adv, 2015, 5(2): 027130.

[25] R U Haq, S Nadeem, Z H Khan, N F M Noor. *Convective heat transfer in MHD slip flow over a stretching surface in the presence of carbon nanotubes*, Physica B: Condens Matter, 2015, 457: 40-47.

[26] M A Chaudhary, J H Merkin. *Free convection boundary layers driven by exothermic surface reactions: critical ambient temperatures*, Math Eng Industry, 1995, 5(2): 129-145.

[27] J H Merkin, I Pop. *Stagnation point flow past a stretching/shrinking sheet driven by Arrhenius kinetics*, Appl Math Comput, 2018, 337: 583-590.

[28] Q Z Xue. *Model for thermal conductivity of carbon nanotube-based composites*, Physica B: Condens Matter, 2005, 368(1-4): 302-307.

[1]Department of Mathematics, Quaid-I-Azam University, Islamabad 44000, Pakistan.
[2]Al-Farabi Kazakh National University, av. al-Farabi 71, 050040, Almaty, Kazakhstan.
[3]Department of Mechanical and Industrial Engineering, College of engineering Majmaah University, Al-Majmaah 11952, Riyadh, Saudi Arabia.
Email: sohail@qau.edu.pk